Neuroblastoma-targeted nanocarriers improve drug delivery and penetration, delay tumor growth and abrogate metastatic diffusion

Neuroblastoma-targeted nanocarriers improve drug delivery and penetration, delay tumor growth and abrogate metastatic diffusion

Irene Cossu[1,#], Gianluca Bottoni[2,#], Monica Loi[1,$], Laura Emionite[3], Alice Bartolini[4], Daniela Di Paolo[1], Chiara Brignole[1], Francesca Piaggio[1], Patrizia Perri[1], Angelina Sacchi[5], Flavio Curnis[5], Maria Cristina Gagliani[6], Silvia Bruno[6], Cecilia Marini[7], Alessandro Gori[8], Renato Longhi[8], Daniele Murgia[9], Angela Rita Sementa[9], Michele Cilli[3], Carlo Tacchetti[6,10], Angelo Corti[5], Gianmario Sambuceti[2], Serena Marchiò[4,11], Mirco Ponzoni[1,*] and Fabio Pastorino[1,*]*

[1]Laboratorio di Oncologia, Istituto G. Gaslini Genoa Italy

[2]Nuclear Medicine Unit, IRCCS Azienda Ospedaliera Universitaria San Martino–IST Istituto Nazionale per la Ricerca sul Cancro, Genoa, Italy

[3]Animal Facility, IRCCS Azienda Ospedaliera Universitaria San Martino–IST Istituto Nazionale per la Ricerca sul Cancro, Genoa, Italy

[4]Laboratory of Tumor Microenvironment, Candiolo Cancer Institute-IRCCS, Candiolo, Italy

[5]Division of Experimental Oncology San Raffaele Scientific Institute, Milan, Italy

[6]Department of Experimental Medicine University of Genoa, Genoa, Italy

[7]Genoa Section, CNR Institute of Bioimages and Molecular Physiology, Milan, Italy

[8]Istituto di Chimica del Riconoscimento Molecolare, CNR, Milan, Italy

[9]Department of Pathology, Istituto G. Gaslini, Genoa, Italy

[10]Experimental Imaging Center, Scientific Institute San Raffaele, Milan, Italy

[11]Department of Oncology, University of Torino, Italy

[#]sharing first authorship; [*]sharing last authorship

[$]Present address: Department of Viral Immunobiology, Institute of Experimental Immunology, University of Zürich, Zürich, Switzerland.

Corresponding authors: Fabio Pastorino, Ph.D. and Mirco Ponzoni, Ph.D., Laboratorio di Oncologia, Istituto G. Gaslini, Via G. Gaslini 5, 16147-Genoa, Italy. Phone: +3901056363533; Fax: +390103779820. emails: fabiopastorino@ospedale-gaslini.ge.it; mircoponzoni@ospedale-gaslini.ge.it

Keywords:

ABSTRACT

Selective tumor targeting is expected to enhance drug delivery and to decrease toxicity, resulting in an improved therapeutic index. Such an approach might provide a chance for successful therapy, especially for difficult-to-treat tumors. We have recently identified the HSYWLRS peptide sequence as a specific ligand for aggressive neuroblastoma, a childhood tumor mostly refractory to current therapies. Here we validated the specific binding of HSYWLRS to neuroblastoma cell suspensions obtained either from cell lines, animal models, or Schwannian-stroma poor, poorly differentiated, stage IV neuroblastoma patients. Binding of the biotinylated peptide, as well as of HSYWLRS-functionalized fluorescent quantum dots or liposomal nanoparticles was dose-dependent and was specifically inhibited by an excess of free peptide. In animal models obtained by the orthotopic implant into the adrenal glands of athymic mice of either MYCN-amplified or MYCN single copy human neuroblastoma cell lines, treatment with the neuroblastoma-targeted, doxorubicin-loaded Stealth Liposomes HSYWLRS-SL[DXR] increased tumor vascular permeability and perfusion, thus enhancing tumor penetration of the drug. This formulation proved to exert a potent antitumor efficacy, as evaluated by bioluminescence imaging and micro-PET, leading to (i) delay of tumor growth paralleled by decreased tumor glucose consumption, and (ii) abrogation of metastatic spreading, accompanied by absence of systemic toxicity and significant increase in the animal life span. Our findings are functional to the design of targeted nanocarriers with potentiated therapeutic efficacy towards the clinical translation.

INTRODUCTION

Neuroblastoma (NB) is the most common and deadly extracranial solid tumor in children, arising from the sympathetic nervous system and accounting for 8-10% of all childhood cancer and 15% of deaths from pediatric tumor (Maris NEJM 2010). The majority of patients have metastatic disease, and most of them progress despite intensive multimodal treatments. Moreover, most anticancer agents are being used at maximally tolerated doses, leading to short- and long-term toxicity in many patients. Recent advances in understanding the molecular pathogenesis of NB have provided considerable insights into the genetic and biochemical mechanisms underlying NB clinical behavior (Cheung NKV Nature Rev Cancer 2013; Maris JM Lancet 2007). These, in turn, allowed to identify genes, proteins and pathways that might represent effective targets for biologically based therapy. Currently, NB therapeutic targets are classified in four categories: i) genes activated by amplification, mutation, translocation or autocrine overexpression; ii) genes inactivated by deletion, mutation or epigenetic silencing; iii) common target genes relevant to NB and other tumors; iv) membrane-associated protein-derived genes expressed on most NBs (Brodeur GM Expert opinion Ther Targets 2014). In particular, antigens exclusively expressed on the surfaces of tumor cells provide an excellent opportunity for targeting. The disialoganglioside GD_2, the norepinephrine transporter (NET), the neuronal cell adhesion molecule NCAM/CD56 and the somatostatin receptor (SSR) represent the most relevant NBs-related molecules exploited for therapeutic approaches (Cheung NV, JCO 2015; Howard JP, Pediatric Blood cancer 2005; Bozzi F, Anticancer Res 2006; Pashankar FD, J Nucl Med. 2005). However, considering the variety of cell types and signaling pathways involved in the crosstalk between the tumor and its microenvironment, it is reasonable to expect that a multi-target approach including receptors peculiar of the microenvironment would lead to a substantially increased therapeutic efficacy. Therefore, the identification of novel targetable receptors is critical for the achievement of innovative therapeutic strategies that may be provided in feasible combination regimens.

By applying a combined *in vitro*/*ex-vivo* phage display strategy, we recently identified novel NB-specific peptide ligands. Among the validated peptides, HSYWLRS emerged as a promising candidate for future pharmacological development in NB therapy (Loi JCR 2013). Here, we demonstrate that a liposomal formulation of doxorubicin, targeted to NB through the HSYWLRS peptide, increases targeting and penetration of the drug into diseased tissues. This results in an attenuation of drug-related side effects, paralleled by a delay in tumor growth and by abrogation of the metastatic spreading.

MATERIALS AND METHODS

Peptides and Cells Lines

The HSYWLRS peptide was synthesized with additional YSHS and GGG sequences at the N- and C-terminal, respectively, and a further C-terminal cysteine residue, resulting in the YSHSHSYWLRSGGGC sequence. The unrelated peptide YSHSLAKALHAGGGC was used as a control (Loi JCR 2013). These two peptides will be referred hereinafter as HSYWLRS and LAKALHA, respectively. Human (GI-LI-N, HTLA-230 and SH-SY5Y) and murine (NXS2) neuroblastoma (NB) cell lines, and human fibroblasts from healthy donors (FIBRO2/93) were grown in complete Dulbecco's Modified Eagle Medium (DMEM) or RPMI-1640 medium, as previously described (Loi M JCR 2010, 2013 and 2014 (trail); Pastorino F Cancer Res NXS2). For *in vivo* imaging, SH-SY5Y cells were also transduced with a retrovirus for the constitutive expression of the firefly luciferase gene, providing the luc-SH-SY5Y cell line (Pastorino F Clin Cancer Res 2008). Cells were tested for mycoplasma contamination and characterized by cell proliferation, morphology evaluation, and multiplex short tandem repeat profiling test.

Human Samples

Samples derived from **S**chwannian**-**stroma poor, poorly differentiated, stage IV NB patients (Patient IDs: 07-B-1239, 07-B-936 and 07-B-2600), were provided by BIT (Integrated Tumor BioBank of Gaslini Institute, Tissue Section), Istituto G. Gaslini, Genoa, Italy. Collection and manipulation of human samples were approved by the Institute's Ethical Committee and informed consent was obtained from each patient in accordance with the Declaration of Helsinki.

Animal Models

Mice were purchased from Harlan Laboratories (Harlan Italy, S. Pietro al Natisone, Italy) and housed under specific pathogen-free conditions. Animals experiments were reviewed and approved by the licensing and ethical committee of the National Cancer Research Institute, Genoa, Italy, and by the Italian Ministry of Health. Five week-old female, athymic mice were anesthetized with ketamine (Imalgene 1000, Merial Italia SpA., Milan, Italy) and xilezine (Xilor 2%, Bio98 Srl, Milan, Italy), subjected to laparotomy, and injected with 1×10^6 GI-LI-N or SH-SY5Y, in the capsule of the left adrenal gland, as previously described (Loi M JCR 2013; Pastorino F Cancer Res 2003). Mice were monitored at least twice a week for evidence of tumor development and quantification of tumor size, and were sacrificed by cervical dislocation under xilezine, at the

appearance of the first signs of poor health, such as abdominal dilation, dehydration, severe weight loss or paraplegia.

Cell Association of Biotinylated Peptides and of Peptide-functionalized Quantum Dots

Biotin-conjugated HSYWLRS or LAKALHA peptides (150 μg/mL) were incubated for 1 h at 4°C with 5×10^5 of i) NB cell lines and fibroblasts, or ii) single cell suspensions from disaggregated tumors (stage IV NB patients or orthotopic NB mouse models). Samples were washed in PBS supplemented with 1% FBS, followed by incubation for 30 min with Cy3-labeled streptavidin ($Cy^{TM}3$-Streptavidin, GE Healthcare). After extensive washing, Cy3-positive cells were counted by flow cytometry (FACS), using a FACScan instrument (Becton-Dickinson Immunocytometry Systems). Results are expressed as mean ratio fluorescence intensity (MRFI) calculated as the mean fluorescence intensity (MFI) of samples incubated with each peptide divided by the MFI of samples incubated with Cy3-streptavidin only.

The capability of HSYWLRS peptide to recognize NB cell lines was then validated with quantum dots (Qdot), as previously showed to represent reliable proof-of-principle nanoparticles (Curnis F et al Cancer Res 2008). Peptide-functionalized fluorescent Qdot (Qdot 605, Life Technologies, Italy) were prepared by surface coupling of HSYWLRS or LAKALHA peptides via Cys-to-MAL interactions, using the sulfo-SMCC cross-linking reagent. Untargeted Qdot were also prepared as negative controls. Binding assays were carried out as follows: 5×10^5 GI-LI-N, HTLA-230 or SH-SY5Y cells were resuspended in 100 μL of DMEM supplemented with 1% FBS and containing HSYWLRS-Qdot, LAKALHA-Qdot, or None-Qdot. After 2 h incubation on ice, cells were washed in DMEM-1% FBS, fixed with 2% formaldehyde in PBS and analyzed by FACS. Results are expressed as geometric mean fluorescence intensity. Competitive binding assays were performed by mixing the indicated doses of peptide-Qdot with escalating amounts of free peptides.

Cell Association and Internalization of Peptide-functionalized Liposomes

Untargeted and targeted Stealth Liposomes (SL) were prepared as described (Pastorino F Cancer Res 2003/2006; Loi M JCR 2010). In the cellular association studies, 1% molar ratio of Top Fluor Cholesterol (Avanti Polar Lipids) was added as fluorescent tracer (FITC labeling). Five $\times 10^5$ GI-LI-N or SH-SY5Y cells were incubated 1 h at 4°C with FITC-labeled, untargeted, HSYWLRS-functionalized or LAKALHA-functionalized SL (700/1400 nmoles of phospholipids (PL)/mL). Samples were washed in PBS-1% FBS, and counted by FACS. Results are expressed as MRFI calculated as the MFI of samples incubated with peptide-functionalized FITC-labeled SL divided by the MFI of untargeted FITC-labeled SL. Competitive binding assays were performed pre-incubating

NB cells with a 100-1000 × molar excess of the corresponding free peptide and results are expressed as percent binding.

For the internalization assay, 1×10^6 GI-LI-N, HTLA-230 or SH-SY5Y cells were incubated for 1 h at 4°C with FITC-labeled untargeted or HSYWLRS-targeted SL (700 nmoles of PL/mL). After washing and cytospin centrifugation, samples were fixed 30 min with 4% PAF in PBS, saturated 40 min in PBS supplemented with 2% BSA and stained with a monoclonal anti-N-CAM antibody (Ab) (mouse anti-CD56, clone 123C3, Invitrogen) to reveal plasma membrane localization. Binding of the primary Ab was detected with a tetramethylrhodamine isothiocyanate (TRITC)-conjugated rabbit anti-mouse (Sigma-Aldrich) and cell nuclei were stained with 4' 6-diamidino-2-phenylindole (DAPI) (Life Technologies). The cellular distribution of liposomal nanocarriers (green), N-CAM (red) and DAPI (blue) fluorescence was analyzed using a laser scanning spectral confocal microscope (TCS SP2-AOBS; Leica Microsystems, Heidelberg, Germany).

In vivo Therapeutic Studies

Mice bearing orthotopic implantation of human NB cells (Pastorino Cancer Res 2003; Marimpietri Clin Cancer Res 2007; Pastorino Frontiers 2013) were treated starting 28 days after tumor cell implant. In the first set of experiment mice, injected with MYCN-amplified GI-LI-N cells, were treated *i.v.*, once a week for 3 weeks. In a second set of experiments, mice implanted with MYCN single copy luc-SH-SY5Y cells, were treated *i.v.*, once a week, for 2 weeks. Treatments consisted of 5 mg/kg of doxorubicin (DXR), either free or encapsulated into untargeted (SL[DXR]) or HSYWLRS-functionalized SL (HSYWLRS-SL[DXR]). DXR was loaded into the nanocarriers as described (Pastorino Cancer Res 2003 Fab). In each experiment, a group of control mice received HEPES-buffered saline. Animals body weight were recorded every two days and survival times were used as the main criterion for determining treatment efficacy.

In vivo Imaging

Inhibition of primary tumor growth and tumor metastasis, tumor glucose consumption and survival times were used as primary endpoints. Luciferase activity associated to the luc-SH-SY5Y cells was visualized *in vivo* by bio-luminescent imaging (BLI, IVIS Caliper Life Sciences, Hopkinton, MA) after a 10-min incubation with 150 µg/mL of D-luciferin (Caliper Life Sciences), as described (Pastorino F Clin Cancer Res 2010). Radionuclide imaging was performed with a dedicated micro-PET system (Albira, Bruker, US), according to a protocol validated in-house (Marini C, Cell Cycle. 2013;12:3490-9. doi: 10.4161/cc.26461; Massollo M. J Nucl Med. 2013;54:259-66. doi: 10.2967/jnumed.112.106666). After intraperitoneal administration of 100 mg/kg ketamine and 10

mg/kg xylazine, mice were weighted and serum glucose levels tested. Animals were positioned within the scanner and 3-4 MBq of fluorodeoxyglucose (FDG) were injected through the tail vein, soon after start of a 50-min list mode acquisition. Acquisition was reconstructed using the following framing rate: 10 x 15 sec, 5 x 30 sec, 2 x 150 sec, 6 x 300 sec, 1 x 600 sec, according to the Maximal Likelihood Expectation Maximization method (MLEM). An experienced observer, in blind, identified a volume of interest (VOI) in the left ventricular chamber to define arterial tracer input function. Tumor glucose consumption (metabolic rate of glucose - MRGlu espressed in nM × min^{-1} × g^{-1}) was estimated according to the Gjedde-Patlak graphical analysis (Patlak, C.S. J. Cereb. Blood Flow Metab. 3, 1-7, 1983) by using a dedicated software (PMOD, Zurich, Switzerland). Briefly, this software utilizes the time concentration curve in the left ventricle as the input function; an algorithm transforms the original tissue activity measurements by fitting the data in each volumetric pixel (voxel) with the slope of the regression line defined by the model. In all cases, lumped constant value was set at 1.Tumors were always recognized in these maps. To measure lesion volumes (mL), the same PMOD software asked operator to identify voxel with the highest MRGlu. The software thus identified cancer outer borders as all surrounding voxels with glucose consumption ≥40% of this value. Total cancer volume was set to consider also the inner lesion core, irrespective from any metabolic evidence of necrosis. Once generated, this cancer VOI was superimposed to the maps of FDG uptake to measure the maximal Standardized Uptake Value (SUV, the most commonly accepted index of tissue FDG uptake) expressed as the fraction of injected tracer dose normalized for body weight.

***In vivo* Systemic Permeability, Perfusion and Tumor Homing Assays**

In each assay, mice orthotopically injected with GI-LI-N cells were treated at day 28 days with a single bolus of DXR (5 mg/kg), encapsulated into untargeted SL or HSYWLRS-targeted SL. Control mice were inoculated with HEPES-buffered saline. For the permeability assay, 1 mg of Evans Blue dye (Sigma-Aldrich) was co-injected; 1 h after, mice were perfused through the heart with PBS supplemented with 1% BSA, followed by collection of tumors and control organs. Evans Blue was extracted as described (Alberici L et al, Cancer Res 73, 2013). In the perfusion analyses, 24 h after treatment mice received an intravenous injection of sterile saline containing the microvasculature dye fluorescein isothiocyanate (FITC)-lectin (*Lycopersicon esculentum* (Tomato), Sigma-Aldrich) (1.25 mg FITC-lectin/kg), as a marker of perfused blood vessels (Murakami M Cancer Res 2013). After another hour, mice were euthanized and tumors resected. Criopreserved tumor sections stained with the endothelial marker CD31 (rat anti-mouse CD31 (PECAM-1), BD Pharmigen) were imaged by fluorescence microscopy. CD31-positive vessels in presence of FITC-

lectin were identified as perfused blood vessels. Morphometric analysis was performed on randomly selected fields every three sections, observed at × 100 magnification with an Olympus photomicroscope, as described (Martinengo C Cancer Res 2014). To evaluate specific tumor homing, mice were sacrificed 24 hours after treatment. The accumulation of DXR was then evaluated by confocal microscopy on cryopreserved tumor samples. Cell nuclei were stained with DAPI.

Statistics

Results are expressed as mean ± Standard Deviation (S.D.). All the analyses were performed with Prism 5 software (GraphPad, La Jolla, CA): two-way analysis of variance (ANOVA) followed by Tukey's Multiple Comparison Test was used to evaluate differences within treatments; survival curves were drawn as Kaplan-Meier Cumulative Proportion Surviving graphs, and corresponding p-values were calculated by the use of the log-rank (Mantel-Cox) test. Asterisks indicate the following p-value ranges: * = $p<0.05$, ** = $p<0.01$, *** = $p<0.001$.

RESULTS

The HSYWLRS peptide is a targeting moiety for NB cells *in vitro* and *ex-vivo*

To evaluate the specificity of the HSYWLRS peptide, normal fibroblasts (FIBRO2/93), human (GI-LI-N, HTLA-230, SH-SY5Y) and murine (NXS2) NB cell lines, and single cell suspension from Schwannian-stroma poor, poorly differentiated, stage IV NB patients (07-B-1239, 07-B-936, 07-B-2600) and from GI-LI-N and SH-SY5Y xenograft models were incubated with biotin-labeled HSYWLRS or LAKALHA peptides. Specific cellular association was quantified by FACS after incubation with Cy3-labeled streptavidin. Compared to LAKALHA, the HSYWLRS peptide significantly recognized all the NB cell lines tested *in vitro*. No binding was observed to FIBRO2/93. More importantly, the HSYWLRS peptide was able to specifically bind, *ex-vivo*, to NB cells derived from both NB patients and NB-bearing tumors, supporting the rationale for *in vivo* preclinical evaluations (Figure 1A).

The cellular association of HSYWLRS-targeted nanoparticles is peptide specific

In a first set of experiments, HSYWLRS or LAKALHA peptides were coupled to fluorescent quantum dots (Qdot) and surface association to GI-LI-N, HTLA-230 or SH-SY5Y cells was assessed by FACS. Qdot lacking the peptide functionalization (None-Qdot) were also tested as negative control. This analysis showed that HSYWLRS-Qdot bound to all the NB cell lines in a

dose-dependent manner. Although the absolute amounts of HSYWLRS-Qdot associated to each cell line were different, in all cases they were significantly higher compared to both LAKALHA-Qdot and None-Qdot (shown for GI-LI-N cells only). In competitive binding experiments performed with the GI-LI-N and HTLA-230 cell lines, the cellular association of HSYWLRS-Qdot was significantly inhibited by an excess of free HSYWLRS peptide, but not by the unrelated LAKALHA (Figure 1C). In contrast, the observed background binding of LAKALHA-Qdot was not inhibited by an excess of either LAKALHA or HSYWLRS peptides (Figure 1C). Taken together, these results confirm the specificity of HSYWLRS-Qdot for the surface of NB cells.

In a second set of experiments, the capability of HSYWLRS peptide to target NB cells when coupled to FITC-labeled SL was also evaluated. Figure 2A shows that HSYWLRS peptide maintains its NB-targeting property when coupled to liposomes (HSYWLRS-SL-FITC), with a significant, concentration-dependent cellular association to GI-LI-N and SH-SY5Y cells, if compared to the binding of LAKALHA-SL-FITC. In accordance with the Qdot experiment results (see Figure 1C), binding of HSYWLRS-SL to NB cells was inhibited only by an excess of HSYWLRS peptide (Figure 2B).

HSYWLRS-targeted liposomes specifically internalize into neuroblastoma cells *in vitro*

To further characterize the interaction between the described peptide ligand and NB cells, the *in vitro* internalization of targeted SL was evaluated. For this purpose, GI-LI-N, HTLA-230 and SH-SY5Y cells were incubated with untargeted SL-FITC or with HSYWLRS-SL-FITC. Cells were fixed and co-stained with a monoclonal antibody specific for the cellular adhesion molecule N-CAM to reveal plasma membrane localization. The localization and the cellular distribution of nanocarriers evaluated by a confocal microscopy confirm the binding specificity and show a selective internalization of HSYWLRS-SL-FITC (Figure 3).

Altogether, the cellular association and internalization results suggest that HSYWLRS-functionalized nanocarriers can be potentially exploited to deliver anticancer agents into NB cells *in vivo.*

NB-targeted liposomes trigger tumor vascular permeability and perfusion, increase DXR penetration into the tumor and show potentiated therapeutic efficacy

The efficacy of HSYWLRS as NB-targeting moiety for drug delivery *in vivo* was investigated using DXR-loaded nanocarriers. Firstly, vascular permeability was evaluated by the Evans Blue assay after injection of NB-bearing mice with vehicle alone (CTR), untargeted, DXR-loaded SL

(SL[DXR]) or HSYWLRS-SL[DXR]. In this assay, none of the controls affected the biodistribution of the albumin-binding Evans Blue dye, while treatment with HSYWLRS-SL[DXR] significantly enhanced extravasation and accumulation of the dye into orthotopically implanted GI-LI-N tumor mass, but not in nontumor tissues (Figure 4A: tumor and healthy liver reported). Moreover, HSYWLRS-SL[DXR] treatment induced a significant increase in tumor blood vessels perfusion, as determined by injection of FITC-lectin into NB-bearing mice and evaluation of specific fluorescent signals by fluorescence microscopy (Figure 4B). The increased in vascular permeability and perfusion was paralleled by an enhanced tumor accumulation of DXR when encapsulated into HSYWLRS-SL, compared to the untargeted liposomal formulation (Figure S1). As a consequence, HSYWLRS-SL[DXR] significantly increased the survival of NB tumor-bearing mice. Noteworthy, HSYWLRS-SL[DXR] treatment was not toxic, as no severe weight loss was detected throughout the therapy (Figure 4C, insert).

NB-targeted nanocarriers delay NB growth, decrease tumor glucose consumption and inhibit cancer spreading

The therapeutic efficacy of NB-targeted SL-mediated drug delivery was extensively investigated in terms of tumor growth and overall survival in animal models of human NB. In these experiments, free DXR was compared to the DXR-encapsulated, HSYWLRS-targeted formulation. Untargeted liposomal DXR was not further investigated since this formulation did not provide any significant benefit over the free drug in orthotopic NB models (Figure 4 and ref Pastorino F et al Cancer Res 2003). Starting at day 28 after orthotopic implant of luc-SH-SY5Y cells, animals were treated *i.v.*, once a week for 2 weeks, with 5 mg/kg of DXR, either free or encapsulated into HSYWLRS-SL. BLI monitoring of tumor growth before (day 20) and after the treatments (day 40) showed that only HSYWLRS-SL[DXR] led to an effective antitumor response (Figure 5A). Compared to control and to free DXR-treated mice, the administration of HSYWLRS-SL[DXR] resulted in a statistically significant lower increment in tumor volume at day 40 compared to pre-treatment (day 20), as well as in a significant increased animal survival.

The antitumor effects of HSYWLRS-SL[DXR] were further validated in the same orthotopic model using a dedicated micro-PET system. Tumor growth was monitored at day 21 (before treatment, T_{21}), 34 (6 days after the first treatment, T_{34}) and 41 (6 days after the second treatment, T_{41}) after tumor challenge. This analysis confirmed that HSYWLRS-SL[DXR] was able to delay tumor growth, (circled in red, Figure 6A) compared to control or free DXR-treated mice. At the end of the treatments, tumor volumes in HSYWLRS-SL[DXR]-treated mice (1.4±0.7 ml) were statistically

smaller compared to those from both control (5.1±0.93 ml) and free DXR-treated animals (3.6±1,4 ml) (Figure 6B).

The observed decrease in tumor size was paralleled by a reduction in tumor glucose consumption. The MRGlu, which was similar in all 3 groups at T_{21} (66±25, 72±7 and 66.18±8 nanoMol/min/g in untreated, free and liposomal DXR, respectively, p=ns) (Figure 6C) significantly increased up to 172±23 and 136±7 (T_{34}) and to 230,79±27 and 182,39±31 (T_{41}) nanoMol/min/g, in control and free DXR-treated mice ($p<0.01$ *vs* T_{21}). This increment was largely reduced by HSYWLRS-SL[DXR] treatment, leading to MRGlu values at T_{34} and T_{41} (95.32±7 and 146,33±12 nanoMol/min/g and) significantly lower if compared to control and free DXR-treated mice (Figure 6C).

Interestingly, the combined analysis of cancer and whole body glucose metabolism confirmed the selectivity of HSYWLRS-SL[DXR] action. Indeed, targeted liposomal DXR did not modify blood clearance of FDG, which was, instead, significantly increased by free DXR (Figure 6D). Although the underlying mechanisms are beyond the scopes of the present study, this finding indicates that DXR modifies the systemic metabolic pattern due either directly or triggering stress-mediated hormonal response. Accordingly, from the pharmacological point of view, this finding strongly supports the concept of a higher tolerability of HSYWLRS-SL[DXR] with respect to conventional (free) drug administration. On the other hand, this finding has a further implication related to PET evaluation of cancer metabolism. In fact, the selective metabolic effect documented by direct measurement of cancer glucose consumption was relatively less evident when conventional maps of FDG uptake (Figure 6A) and SUV values (Figure S2) were analyzed. This somewhat paradoxical finding closely agrees with the response of whole body glucose consumption to free DXR, which might increase FDG sequestration in the normal tissues limiting its availability for cancer uptake and, consequently, smoothing possible differences in ultimate tracer retention measured by SUV. Although this procedure cannot be extended to the clinical workflow for the complexity of its application, this observation confirms the well recognized limitations of SUV in depicting cancer glucose consumption and the advantages offered by dynamic acquisition and compartmental analysis..

Noteworthy, HSYWLRS-SL[DXR] treatment was also able to drastically and totally inhibit NB macrometastases formation (Figure 7A). At T_{41}, free DXR evidenced a partial, significant decrease in the number of tumor metastases compared to control mice. However, no mice treated with HSYWLRS-SL[DXR] evidenced tumor spreading (Figure 7A-B), resulting significantly more potent than free DXR. The number of metastatic lesions was evaluated by inspection. Since this approach has intrinsic limitations due to the limited resolution of positron emission detection associated with the abdominal location of repetitive lesions, the number of metastases was also

directly correlated with total lesion volumes, which strongly documented the effect of HSYWLRS-SL[DXR] against cancer spreading (Figure 7C).

DISCUSSION

In this manuscript we demonstrate that the HSYWLRS peptide is a valuable targeting moiety for drug delivery to human neuroblastoma (NB). We provide evidence that this ligand specifically recognize NB cell lines, as well as single cell suspensions derived from mice xenografts and from biopsies of Schwannian-stroma poor, poorly differentiated, stage IV NB tumors. We also show that a HSYWLRS-functionalized, doxorubicin (DXR)-loaded nanocarriers selectively increases tumor binding and penetration leading to reduced tumor glucose consumption and tumor growth and to the abrogation of metastatic spreading in aggressive orthotopic mouse models of human NB.

NB is the most common extracranial solid tumor in children. Approximately 40% of NB tumors are classified as high-risk and their management includes combinations of chemotherapy, autologous stem cell transplantation, surgery, and radiation therapy. Despite these aggressive treatments, children with high-risk NB have very poor 5-year overall survival rate, due to relapsed and/or treatment-resistant tumors (Maris NEJM 2010). A further increase in therapeutic dose intensity is not feasible, because it will lead to prohibitive short-term and long-term toxicities. New approaches with targeted therapies may improve efficacy and decrease toxicity (Matthay Clin Cancer Res 2012).

Nanotechnology offers potential developments in pharmaceutical, medical imaging and diagnosis and cancer treatment (Etheridge ML Nanomedicine, Nanotechnology, Biology and Medicine 2013). In clinical applications, drug-loaded nanocarriers, like liposomes, have been pursued especially because they passively accumulate at sites of increased vascular permeability and because encapsulation reduces the side effects usually associated to free drugs. These features result in an overall increase of the therapeutic index (efficacy over toxicity); however, due to the poor extravasation of liposomes into solid tumors with tight endothelial junctions, the gain in therapeutic index has been more on the side of reduced toxicity than on that of increased efficacy (Allen TM Advanced Drug Delivery Reviews 2013).

Here, we demonstrate that, compared to untargeted nanocarriers, our HSYWLRS-targeted, DXR-loaded liposomal formulation was able to increase tumor vascular permeability and perfusion, leading to an higher DXR accumulation into the neoplastic mass and, as a consequence, to an increased therapeutic effect (Figure 4 and S1 supplementary). No long term survivors were, however, achieved from our experimental therapy. Commonly, the use of nanoparticles to treat solid tumors does not enable uniform delivery of the encapsulated drug to all regions of tumors as a

result of physiological barriers presented by the abnormal tumor vasculature and interstitial matrix (Vakoc BJ, Nat Med 2009). However, the results here obtained encouragingly allow to hypothesize that a therapeutic strategy based, for instance, on tumor vasculature normalization (Jain RK, Nat Rev Clin Oncol 2010) and on the use of more penetrating, targeted-liposomes, might help drug-loaded nanoparticles to penetrate faster and deeper inside the tumor (Sugahara KN Cancer Cell 2009).

Being an approximation of reality, mouse models of cancer are critical for the development of new and more effective antitumor therapies. Therefore, it is of notable importance to have orthotopic systems that can mimic the tumor biology observed in patients and give accurate information on the signaling networks involved in the tumor microenvironment (Talmadge JE, Am J Pathol. 2007; Loi M The International Journal of Developmental Biology 2011). Taking into account that MYCN gene status is one of the strongest determinant of NB patients clinical outcome (Cohn S JCO 2009), in this work MYCN amplified and MYCN single copy human NB cells were orthotopically injected in the adrenal glands of mice. The results obtained show that HSYWLRS-targeted, DXR-loaded liposomes exerted a dramatic antitumor effect, leading to a significant increase in life span, in both mouse models used (Figures 4C and 5C).

Furthermore, in contrast to other experiments, in which NB-bearing mice received targeted, DXR-loaded nanocarriers after 4 h, or after 1, 5, 10 or 21 days post tumor cells inoculation (Loi M JCR 2013; Pastorino Cancer Res 2003 Fab; Pastorino Cancer res 2006), in this work we decided to start dosing the mice 4 weeks after tumor cells challenge to emphasize the potential of our novel targeted therapy against aggressive and well established NB tumors.

In this manuscript we also describe novel imaging protocols for more accurate evaluation of NB progression in animal models. The use of bioluminescent imaging (BLI) for the detection of cancer growth in preclinical studies is well-documented (O'Neill K, J Pathol. 2010). In xenograft models, the growth of luciferase-expressing tumor cells can be monitored by real-time, non-invasive imaging in live animals over time. However, while representing an useful technique during early stages of tumor onset, in our opinion BLI looses sensitivity upon tumor progression, with the luminescent signal reaching saturation and making it difficult to quantify the exponential tumor growth and the effectiveness of treatments. In the mouse model used in this study, BLI was unable to detect tumor metastases, likely because the high signal from primary tumors overcame the weak luminescence from potential small foci at distant organs. For these reasons, we evaluated NB progression by using a high-resolution small animal PET scanner. Recently, Quarta et al. reported the value of FDG imaging with micro-PET for the detection of spontaneously growing NB in TH-MYCN transgenic mice (Quarta C Mol Imaging Biol 2013). Our measurements of FDG uptake in

the orthotopic tumor model provided results remarkably similar to that study. However, we extended that preliminary experience reporting that FDG SUV alone is a relatively inaccurate index of tumor response to treatment. The uptake of this tracer is directly correlated to cancer glucose avidity and inversely correlated to the glucose greed of the whole body (Marini Cell Cycle 2013). In this line, the finding of increased FDG clearance rate in mice treated with free DXR has a two-fold implication. From a pharmacodynamic point of view, this indicates that free DXR causes a more prominent systemic reaction compared to encapsulated DXR, thus suggesting higher drug interaction with non-target tissues (Figure 6D). In turn, the higher sequestration of the tracer in normal tissues eventually causes a decrease of its bioavailability for tumor uptake, limiting the accuracy of SUV as an index of lesion glucose disposal (Massollo M. J Nucl Med. 2013;54:259-66. doi: 10.2967/jnumed.112.106666). We therefore extended the clinical analysis of FDG uptake using standardized compartmental approach to quantitatively estimate NB glucose consumption, thus confirming the well-documented relationship between glycolytic flux and cancer proliferation rate (Marini Cell cycle 2013). The results of this analysis showed that HSYWLRS-SL[DXR] has a potent effect on cancer growth that is preceded by an evident and persisting reduction in MRGlu (Figure 6). Overcoming the limitations of BLI, the micro-PET imaging also allowed the evaluation of metastases, an extremely important feature being metastases the major cause of death for cancer patients (Nguyen, D.X. Nat Rev Cancer 2009). Remarkably, treatment with HSYWLRS-SL[DXR] completely abrogated NB tumor spreading (Figure 7), paving the way to its clinical development.

As a note of caution, it is becoming evident that cells cultured *in vitro* before their injection in animals might develop aberrant and irreversible genetic and phenotypic changes, not consistent with the properties of the original patient tumors (Tentler JJ et al, Nat Rev Clin Oncol 2012). Consequently, the use of i) NB transgenic animals (Teitz T Cancer Res 2013); ii) transplantable TH-MYCN tumor model in syngenic mice (Kroesen M Int J Cancer 2014); iii) NB patient-derived xenografts (PDXs) by implantation of viable tumor explants from cancer patients (Braekeveldt N Int J Cancer 2014) would be an extremely valid approach for further resemble clinically relevant NB tumors, maintaining patient-derived tumor cells characteristics.

Finally, our novel NB-targeted system could be part of simultaneous or sequential multi-target approaches that exploit receptors expressed on the tumor microenvironment (*i.e.* the endothelial cell marker Aminopeptidase N (Pastorino Cancer res 2003), the perivascular cell marker Aminopeptidase A (Marchiò Cancer Cell 2004; Loi M JCR 2010)), and on the tumor cells themselves (*i.e.* GD_2 (Pastorino Frontiers Oncol 2013)). Such an approach, in principle, may promote synergistic targeting effects, and therefore potentiate the therapeutic response to the described nanodrugs.

REFERENCES

GRANT SUPPORT

Associazione Italiana per la Ricerca sul Cancro (AIRC) My First AIRC Grant, (MFAG) (FP and SM), and AIRC-IG 14231 (MP); Fondazione Umberto Veronesi (FUV) (FP and CB).

ACKNOWLEDGMENTS

FP is supported by FUV and Istituto G. Gaslini (IGG) Award 2013-2014. AB is a recipient of Fondazione Piemontese per la Ricerca sul Cancro (FPRC) fellowship. ML is a recipient of a Fondazione Italiana per la Ricerca sul Cancro (FIRC) fellowship; DDP and FP are a recipient of a FUV fellowship. PP is supported by IGG Award 2014-2015.We thank BIT (Integrated Tumor BioBank of Gaslini Institute, Tissue Section), Istituto G. Gaslini, Genoa, Italy for providing the human tumor samples.

LEGENDS

Figure 1. The **HSYWLRS peptide is a ligand for NB cells. A)** Specific binding *in vitro* to human (GI-LI-N, HTLA-230, SH-SY5Y) and murine (NXS2) NB cell lines, and *ex vivo* to NB cells derived from human samples (07-B-1239, 07-B-936 and 07-B-2600) of stage IV, NB patients and from orthotopically injected tumor-bearing mice (xenograft GI-LI-N and SH-SY5Y); no binding to healthy human fibroblasts (FIBRO2/93). Biotin-conjugated HSYWLRS or LAKALHA (unrelated) peptides (150 µg/mL) were incubated with 1×10^6 cells for 1 h at 4°C, followed by incubation for 30 min with Cy3-labeled streptavidin. Cy3-positive cells were counted by flow cytometry (FACS). Columns: MRFI ± S.D. **, $p < 0.01$ and ***, $p < 0.001$: HSYWLRS *vs* LAKALHA. **B-C)** HSYWLRS-Qdot specifically bind to NB cell lines. Direct binding **(B)** and competitive binding **(C)** assays of peptide-Qdot conjugate to GI-LI-N, HTLA-230 and SH-SY5Y cell lines. Binding assays were performed as follows: 5×10^5 cells were resuspended in a solution containing HSYWLRS-Qdot or LAKALHA-Qdot, or None-Qdot in DMEM-1% FBS incubated for 2 h on ice. Competitive binding assays were performed by mixing the indicated dose of peptide-Qdot conjugate with escalating amounts of free peptide. Cells were fixed in 2% formaldehyde in PBS and analyzed by FACS. **, $p < 0.01$: HSYWLRS-Qdot *vs* LAKALHA-Qdot.

Figure 2. HSYWLRS-functionalized liposomes specifically bind NB cells *in vitro*. A) 1×10^6 GI-LI-N or SH-SY5Y cells were incubated for 1 h at 4°C with FITC-labeled untargeted SL or with FITC-labeled HSYWLRS- or LAKALHA-SL (700/1400 nmoles of phospholipids (PL)/mL). **B)** GI-LI-N and SH-SY5Y cells were incubated with FITC-labeled HSYWLRS- or LAKALHA-SL (1400 nmoles of phospholipids (PL)/mL), either alone or in combination with a molar excess (100-1000 ×) of free peptide. Samples were analyzed by FACS. Columns: MRFI ± S.D. The results of the competition experiments are expressed as percent binding. **A)** *, $p < 0.05$; **, $p < 0.01$; ***, $p < 0.001$: HSYWLRS-SL-FITC *vs* LAKALHA-SL-FITC . **B)** ***, $p < 0.001$: HSYWLRS 100x and 1000x HSYWLRS-SL-FITC *vs* HSYWLRS-SL-FITC.

Figure 3. HSYWLRS-functionalized liposomes are specifically internalized by NB cells. 1×10^6 GI-LI-N, HTLA-230 or SH-SY5Y were incubated for 1 h at 4°C with FITC-labeled untargeted liposomes (SL) or with FITC-labeled HSYWLRS-targeted SL (700 nmoles of phospholipids (PL)/ml). After washing, samples were fixed and stained with an anti-NCAM monoclonal antibody

for plasma membrane localization. Binding of the primary antibody was detected with a PE-conjugated rabbit anti-mouse antibody, and cell nuclei were stained with DAPI. Fluorescence was analyzed with a laser scanning spectral confocal microscope. Liposomes are shown in green, N-CAM in red and DAPI in blue. Scale bar = 50 μm.

Figure 4. Treatment with HSYWLRS-functionalized, DXR-loaded liposomes induces tumor permeability and perfusion, and increases life span of MYCN-amplified GI-LI-N-bearing mice. A) *In vivo* systemic permeability. Mice (n=3/group) orthotopically injected with GI-LI-N cells were treated, 28 days after, with a single bolus of DXR (5mg/kg), encapsulated into untargeted (SL[DXR]) or HSYWLRS-targeted (HSYWLRS-SL[DXR]) liposomes, in combination with 1 mg of Evans Blue dye. Control mice (CTR) received HEPES-buffered saline. After 1 h circulation, mice were perfused, tumors and livers collected and Evans Blue extracted and quantified (O.D. 600 nm). Results are expressed as Evans Blue dye for gram of tissue. **, $p < 0.01$: HSYWLRS-SL[DXR] *vs* CTR and SL[DXR]. **B)** Exemplary GI-LI-N tumor sections from control mice or from mice treated with SL[DXR] or HSYWLRS-SL[DXR] and inoculated with FITC-lectin (green). Red: CD31. Blue: cell nuclei (DAPI). Scale bar: 40 μm. Right side, mean number of FITC-lectin positive cells ± SD. ***, $p < 0.001$, HSYWLRS-SL[DXR] *vs* CTR and SL[DXR]. **C)** DXR-loaoded liposomes functionalized with HSYWLRS peptide show potentiated therapeutic efficacy. Mice (n=8/group) orthotopically injected with GI-LI-N cells were treated *i.v.*, once a week for 3 weeks, with 5 mg/kg of DXR, either free (free DXR) or encapsulated into SL[DXR] or HSYWLRS-SL[DXR] liposomes. Control mice received Hepes buffer saline only (CTR). Survival: $p = 0.0008$: HSYWLRS-SL[DXR] *vs* SL[DXR]). Insert: mean body weight after treatments. Arrows: days of treatment post tumor cell inoculation.

Figure 5. Treatment with HSYWLRS-functionalized, DXR-loaded liposomes delays tumor growth as evaluated by BLI and increases life span in MYCN single copy SH-SY5Y tumor model. A) Lateral (cell implantation side) images from mice orthotopically injected with luc-SH-SY5Y cells. Animals (n=4/CTR; n=5/treatments) were treated *i.v.*, once a week for 2 weeks, with 5 mg/kg of DXR, either free (free DXR) or encapsulated into HSYWLRS-targeted liposomes (HSYWLRS-SL[DXR]). Control (CTR) mice (n=4) received HEPES-buffered saline. Tumor growth was monitored by BLI at day 20 (before treatment) and 40 (end of treatments) after tumor challenge. **B)** Antitumor effects at the end of treatments; the values into the ROIs are reported as fold increase in tumor volume at day 40 over day 20. Columns: mean of tumor fold increase ± S.D.

*, $p < 0.05$: free DXR *vs* CTR; **, $p < 0.01$: HSYWLRS-SL[DXR] *vs* free DXR; ***, $p < 0.001$: HSYWLRS-SL[DXR] *vs* CTR; **C)** DXR-loaded liposomes functionalized with HSYWLRS peptide show potentiated therapeutic efficacy. Survival: $p = 0.0025$: HSYWLRS-SL[DXR] *vs* CTR and free DXR. Arrows: days of treatment post tumor cells inoculation.

Figure 6. Treatment with HSYWLRS-functionalized, DXR-loaded liposomes delays tumor growth, decreases tumor glucose consumption and abrogates metastatic spreading as evaluated by micro-PET. Mice (n=4/CTR; n=5/treatments) orthotopically implanted with luc-SH-SY5Y cells were treated as reported in legend of Figure 5. For the micro-PET analysis, a bolus of 3-6MBq-fluorodeoxyglucose (FDG) was injected via the tail vein during a 1-h list mode acquisition. After framing rate optimization, tumor glucose consumption was measured at T_{21} (before treatment), T_{34} (6 d after the first treatment) and T_{41} (6 d after the second treatment) after tumor challenge. **A)** micro-PET images. 1: FdG uptake map; 2: Glucose consumption map; a: transaxial section; b: sagittal section; c: coronal section. Red circle: tumor masses. **B-D)** Tumor volume, MRGLu and FDG clearance at the indicated time points. Arrows: days of treatment post tumor cell inoculation. **B)** Delay of tumor growth in HSYWLRS-SL[DXR]-treated mice. Each point: mean ± S.D. T_{34}: ***, $p < 0.001$: HSYWLRS-SL[DXR] *vs* control; T_{41}: ***, $p < 0.001$ and **, $p < 0.01$: HSYWLRS-SL[DXR] *vs* control and *vs* free DXR, respectively. **C)** Reduction of tumor glucose consumption in HSYWLRS-SL[DXR]-treated mice. T_{34}: ***, $p < 0.001$: HSYWLRS-SL[DXR] *vs* control and free DXR; T_{41}: ***, $p < 0.001$: HSYWLRS-SL[DXR] *vs* control; *, $p < 0.05$: HSYWLRS-SL[DXR] *vs* free DXR. **D)** FDG clearance. Increased FDG clearance in free DXR-treated mice. *, $p < 0.05$: free DXR *vs* control and HSYWLRS-SL[DXR].

Figure 7. Treatment with HSYWLRS-functionalized, DXR-loaded liposomes inhibits tumor spreading. Mice (n=4/CTR; n=5/treatments) orthotopically implanted with luc-SH-SY5Y cells were treated as reported in legend of Figure 5 and evaluated by PET at T_{41} as in Figure 6. **A)** Glucose consumption maps (white arrows: primary tumor; black arrows: metastases). **B-C)** Number and volume of metastases, respectively. Columns: means ± S.D. *, $p < 0.05$: free DXR *vs* CTR; **, $p < 0.01$: HSYWLRS-SL[DXR] *vs* free DXR; ***, $p < 0.001$: HSYWLRS-SL[DXR] *vs* CTR.

Supplementary Legends

Figure S1. DRX-loaded liposomes targeted to NB through the HSYWLRS-peptide enhance tumor drug accumulation. Tumor homing of HSYWLRS-SL[DXR] was evaluated following *i.v.* administration into mice bearing human GI-LI-N-derived orthotopic xenografts (n=3/group). The accumulation of DXR (red) was evaluated by confocal microscopy on cryopreserved tumors derived from CTR or from SL[DXR]- or HSYWLRS-SL[DXR]-treated mice. Blue: cell nuclei (DAPI). Scale bar: 100 μm.

Figure S2. SUV index evaluated by micro-PET. Mice (n=4/CTR; n=5/treatments) orthotopically implanted with luc-SH-SY5Y cells were treated as reported in legend of Figure 5 and evaluated by PET at T_{21}, T_{34} and T_{41}. No significant differences in maximal Standardized Uptake Volume (SUV) were observed between the different groups of treatment.

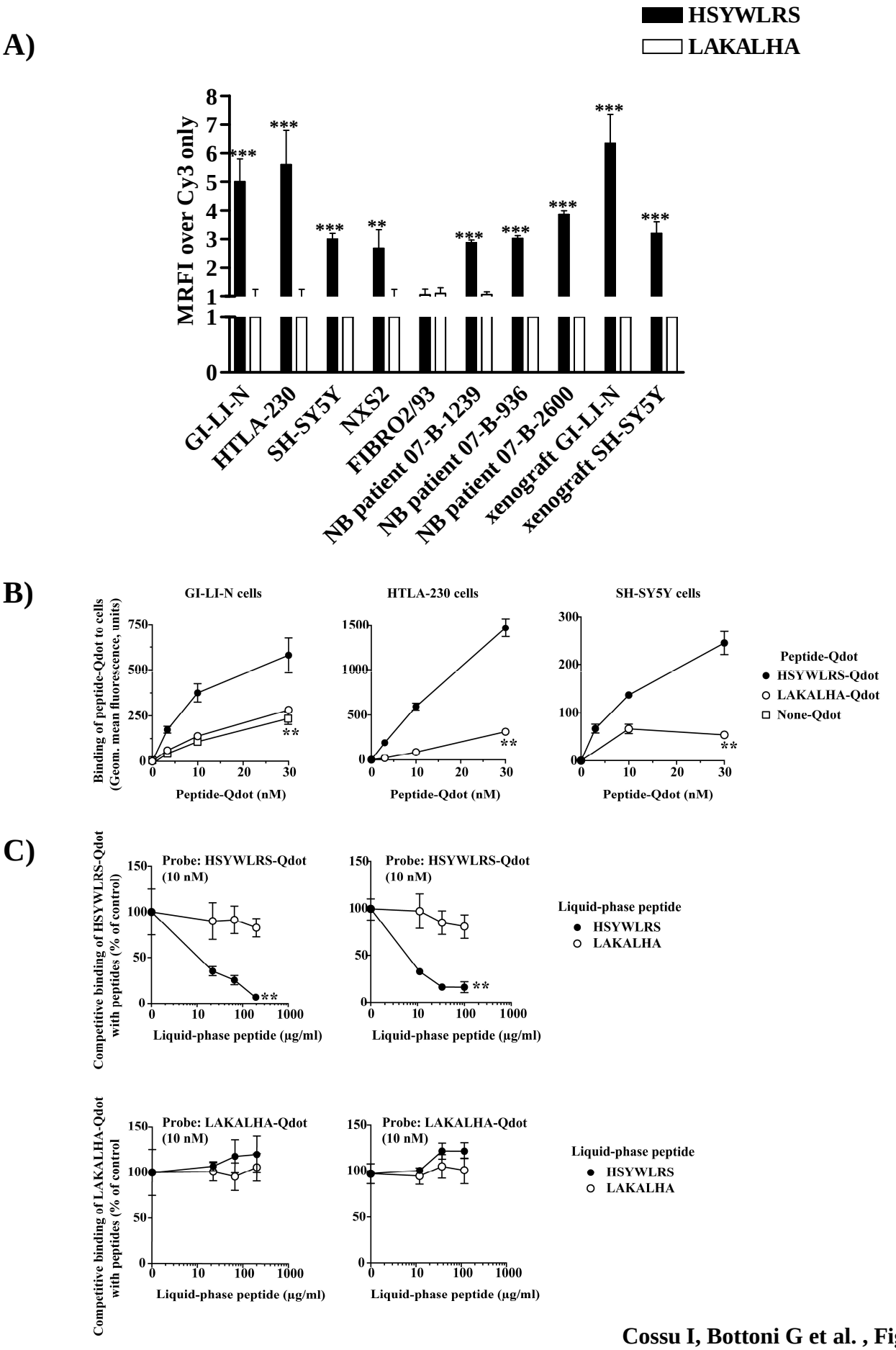

Cossu I, Bottoni G et al. , Figure 1

A)

GI-LI-N cells

SH-SY5Y cells

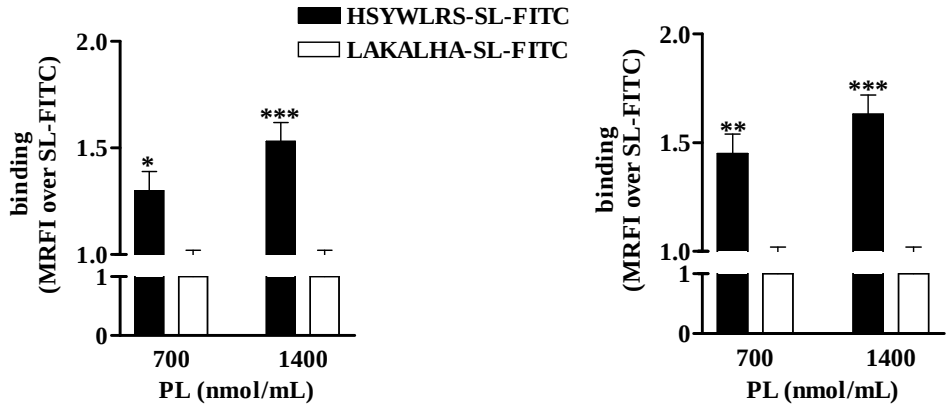

B)

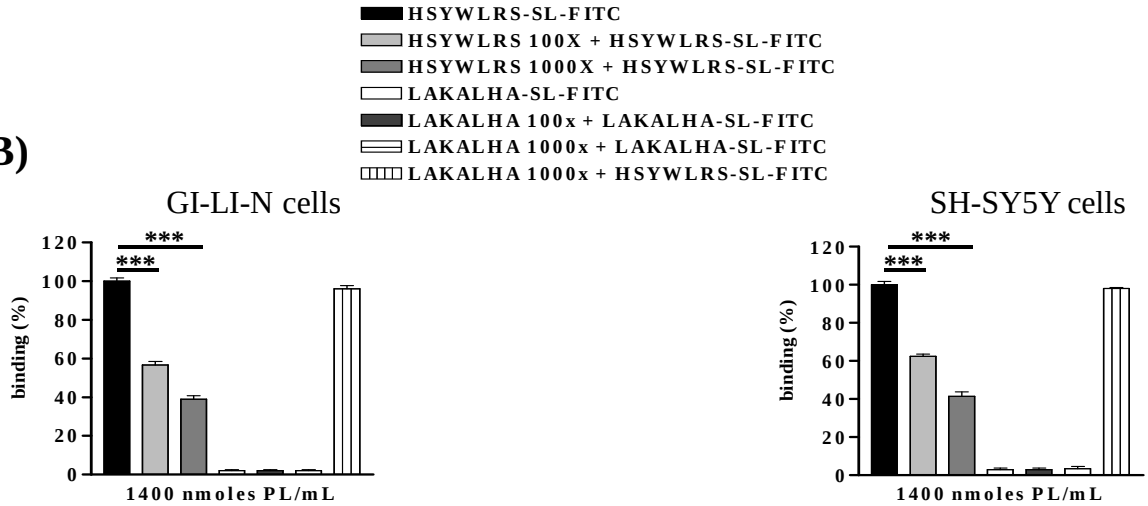

Cossu I, Bottoni G et al. , Figure 2

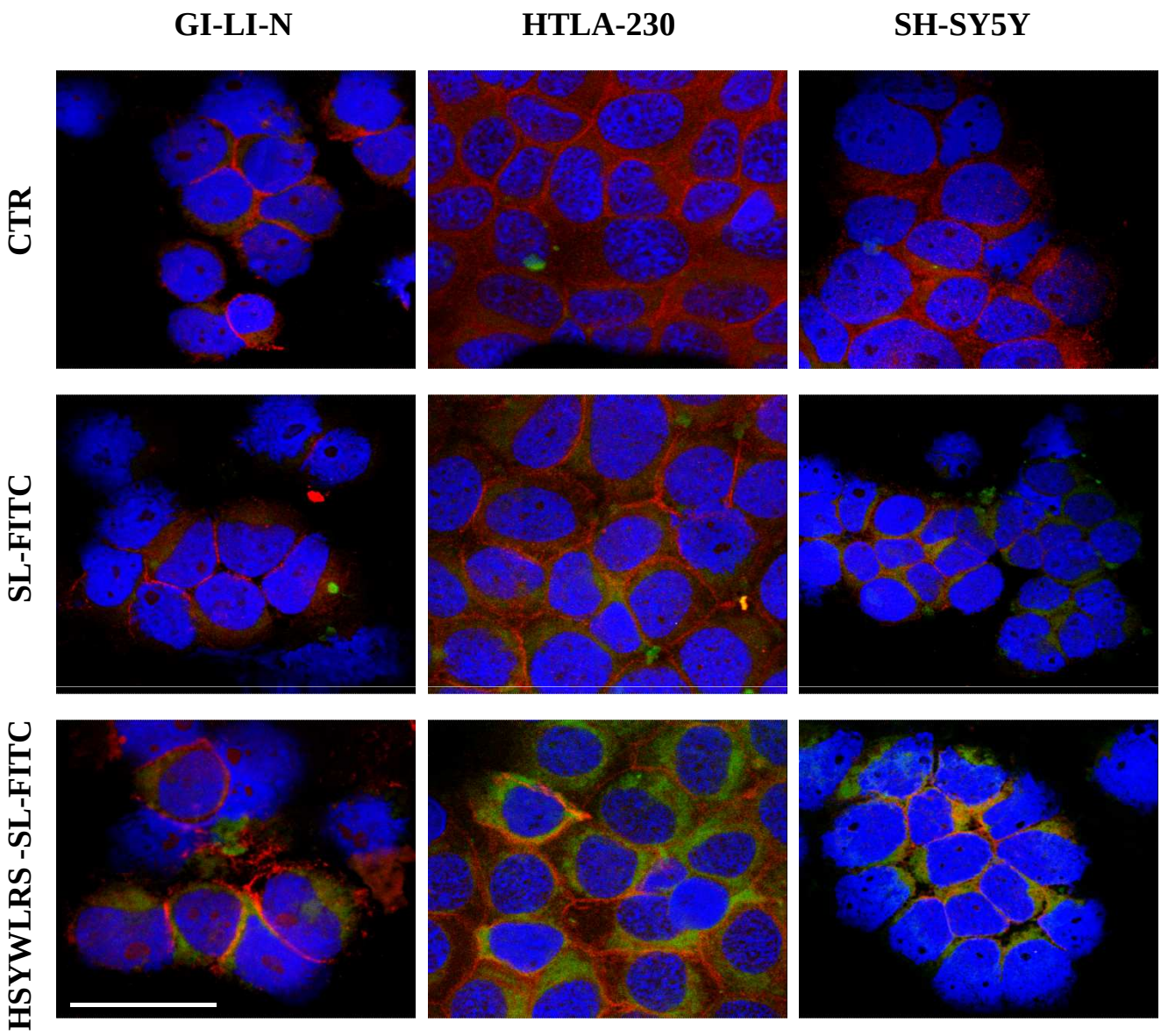

Cossu I, Bottoni G et al. , Figure 3

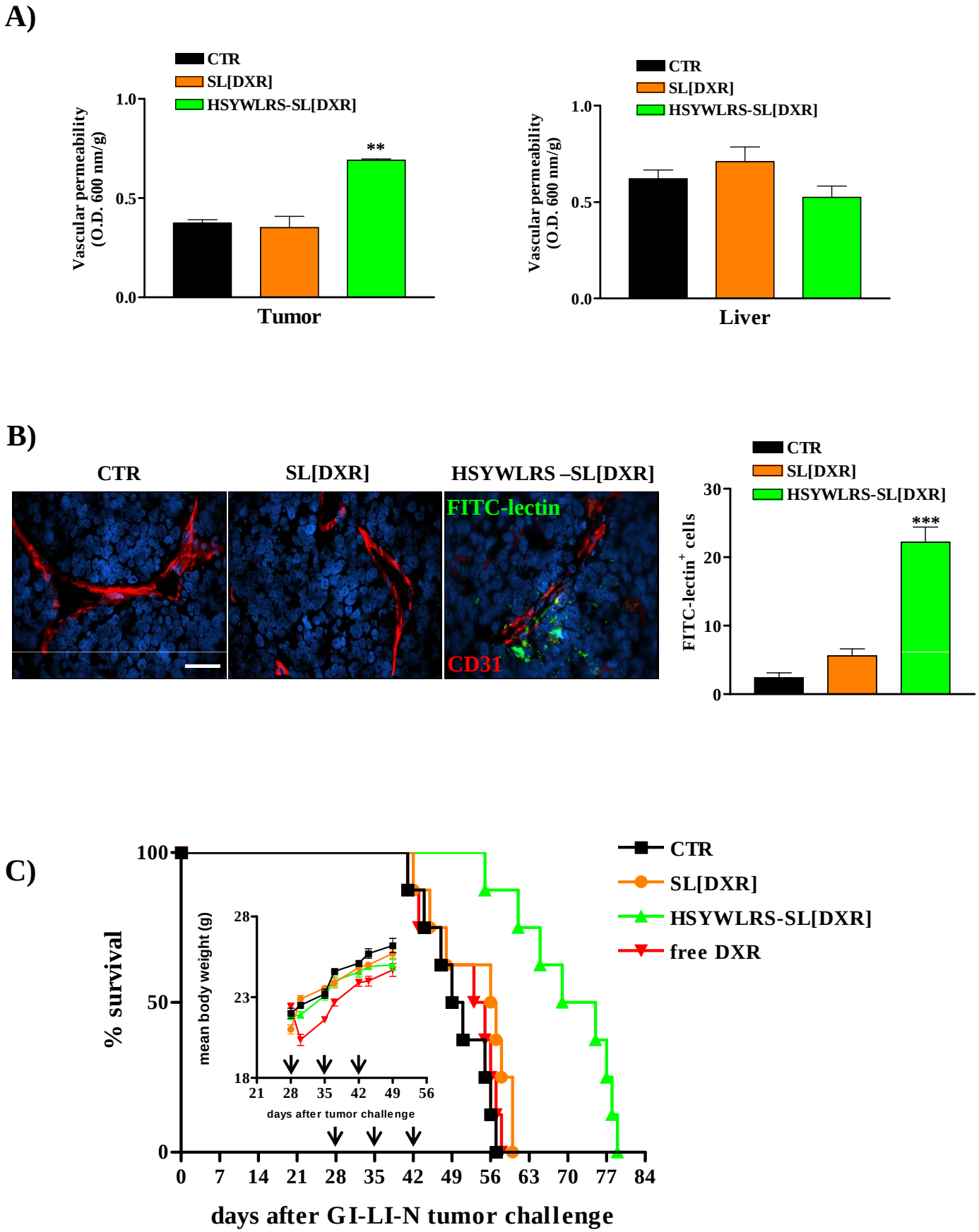

Cossu I, Bottoni G et al. , Figure 4

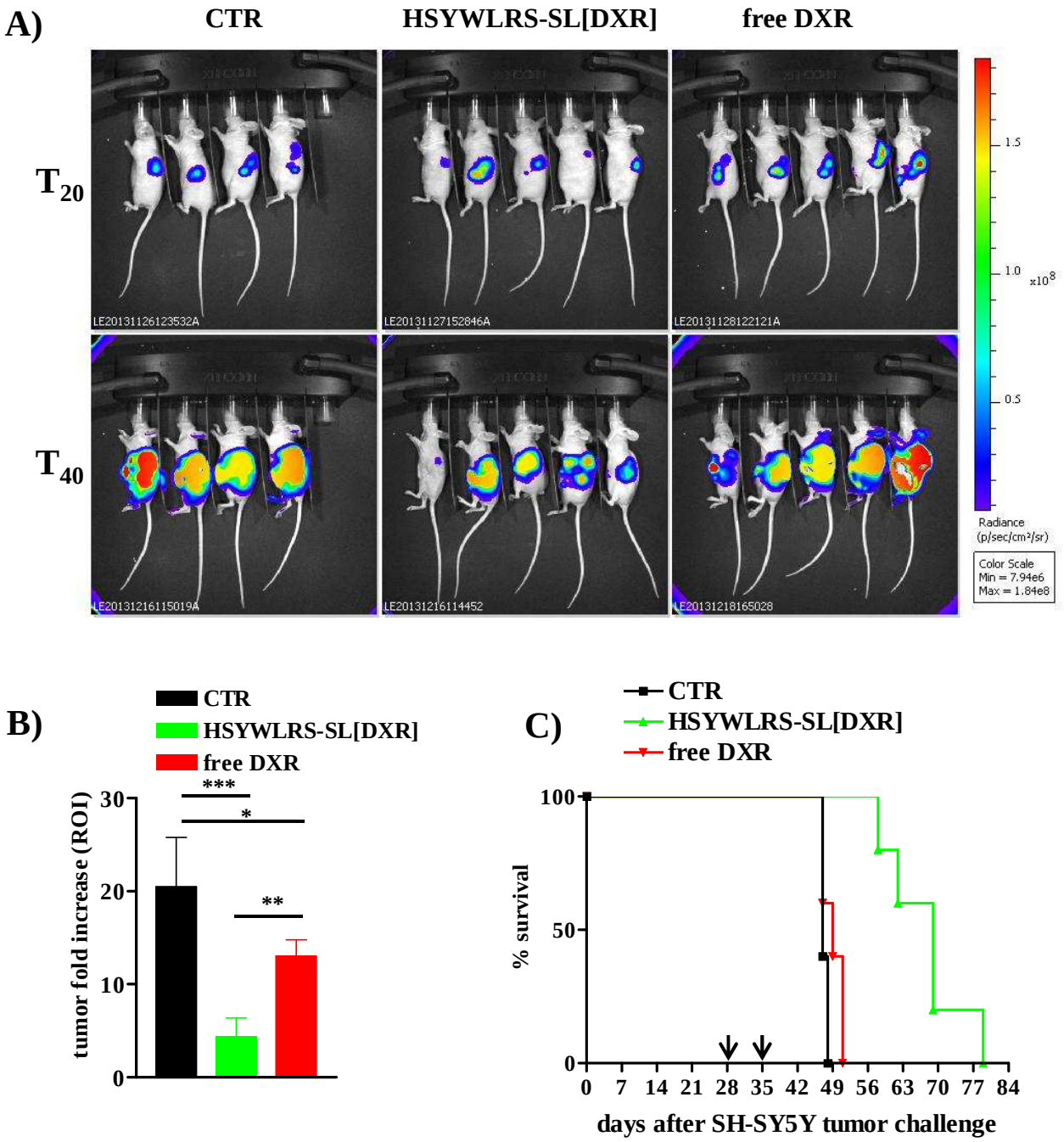

Cossu I, Bottoni G et al. , Figure 5

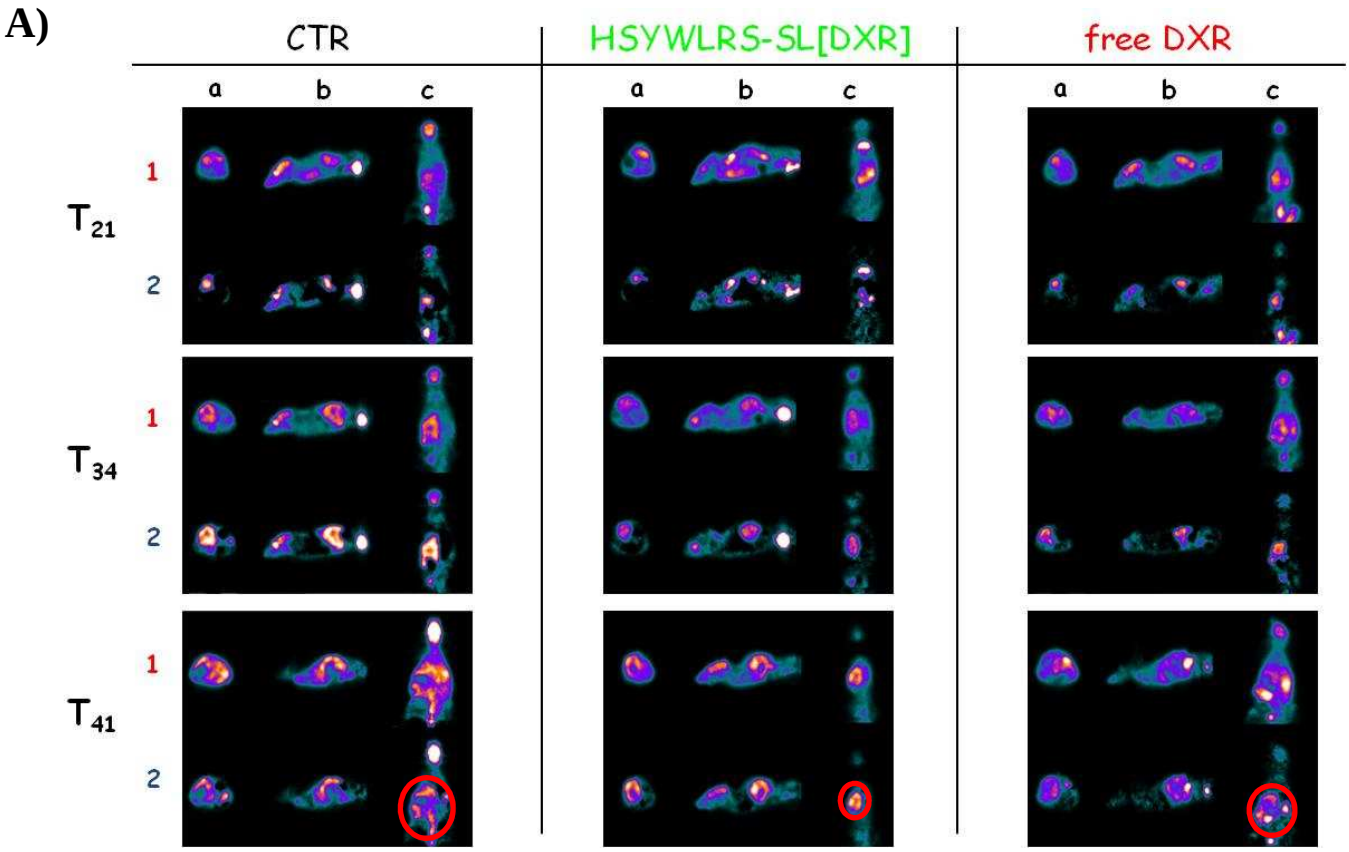

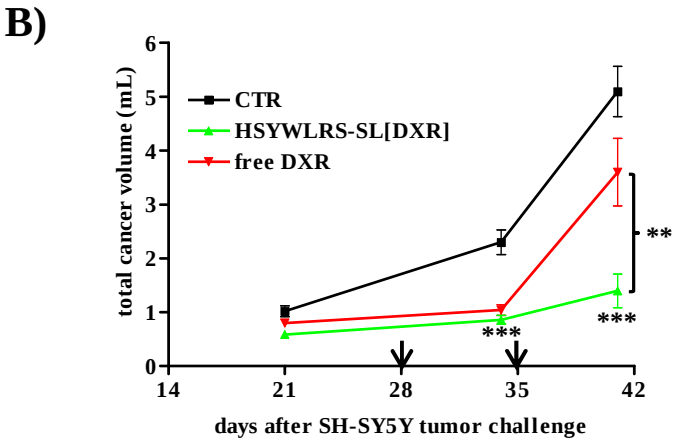

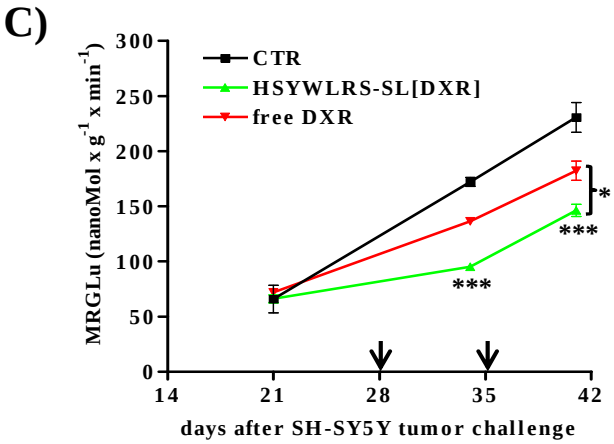

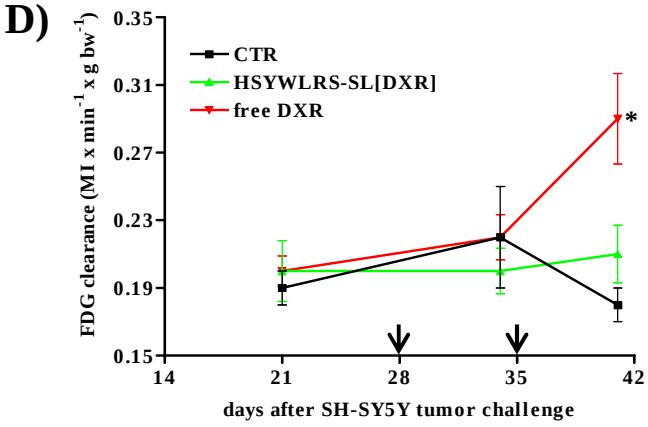

Cossu I, Bottoni G et al. , Figure 6

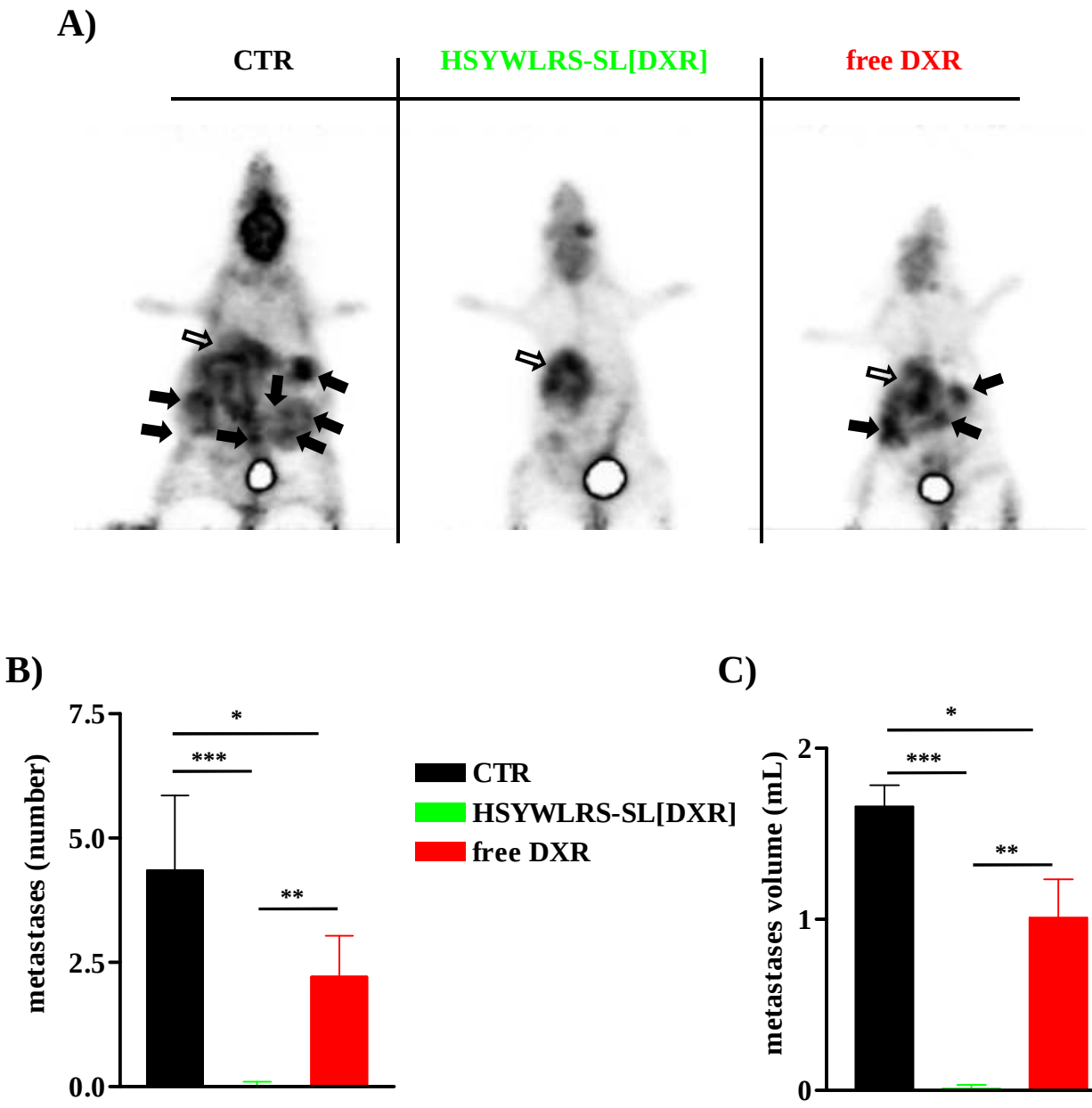

Cossu I, Bottoni G et al. , Figure 7

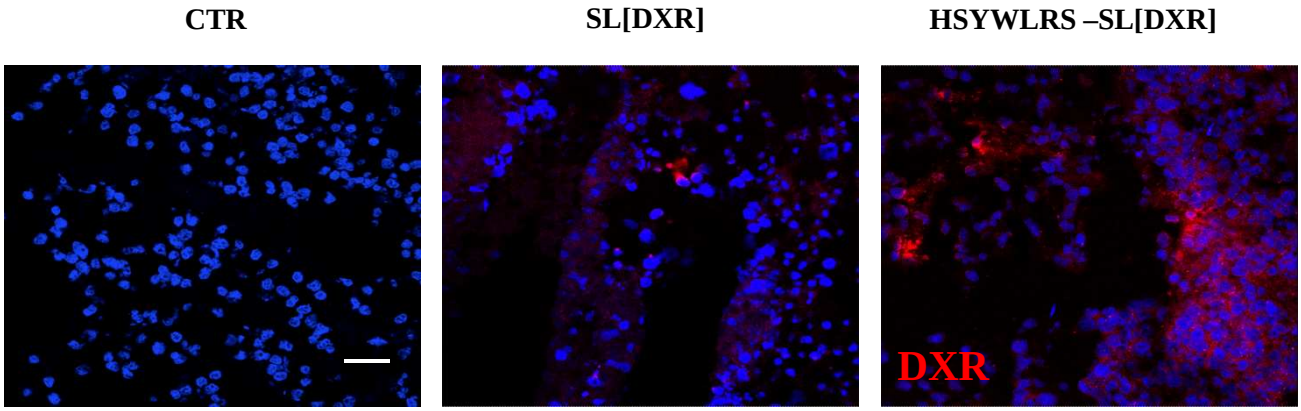

Cossu I, Bottoni G et al. , Figure S1

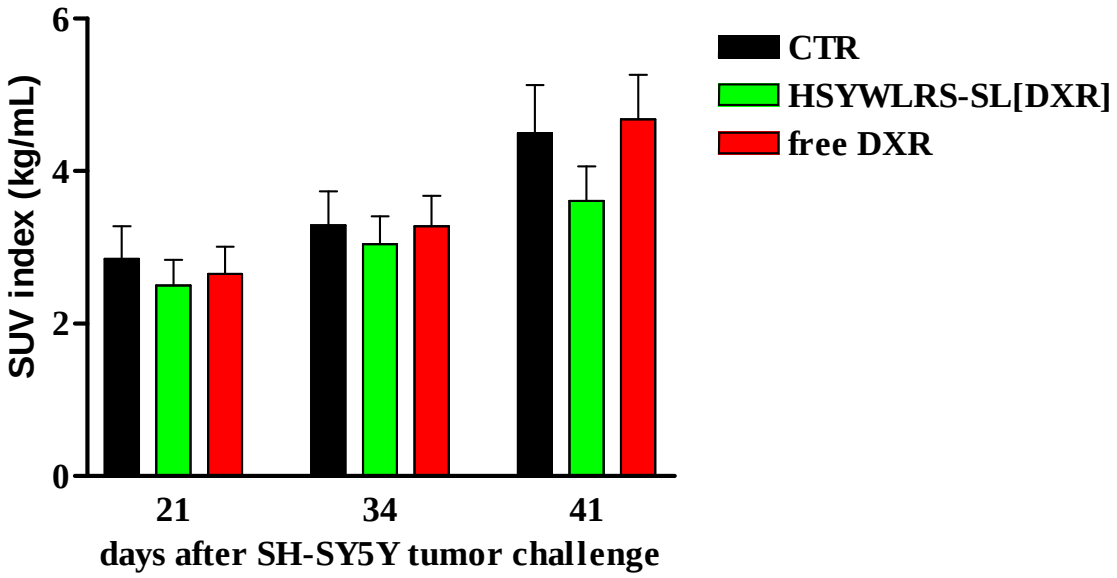

Cossu I, Bottoni G et al. , Figure S2